Information propagation in a noisy gene cascade

D. Monteoliva*
Departamento de Física, Facultad de Ciencias Exactas, Universidad Nacional de La Plata, Argentine

L. Diambra†
Centro Regional de Estudios Genómicos, Universidad Nacional de La Plata, CONICET, Argentine
(Received 17 February 2017; revised manuscript received 1 June 2017; published 5 July 2017)

We use information theory to study the information transmission through a simple gene cascade where the product of an unregulated gene regulates the expression activity of a cooperative genetic switch. While the input signal is provided by the upstream gene with two states, we consider that the expression of downstream gene is controlled by a *cis*-regulatory system with three binding sites for the regulator product, which can bind cooperatively. By computing exactly the associated probability distributions, we estimate information transmission thought the mutual information measure. We found that the mutual information associated with unimodal input signal is lower than the associated with bimodal inputs. We also observe that mutual information presents a maximum in the cooperativity intensity, and the position of this maximum depends on the kinetic rates of the promoter. Furthermore, we found that the bursting dynamics of the input signal can enhance the information transmission capacity.

DOI: 10.1103/PhysRevE.96.012403

I. INTRODUCTION

The cells membranes are continuously bombarded by external molecular signals. Signaling networks control the flow of this information from cell membrane to the nucleus. This control takes place through several covalent modification cycles (kinase-phophatase cascades), which are able to filter out noise, amplify weak signals, modulate the dynamic range, or allow alternative regulatory entry points for information flow [1]. Thus, the structure of the signal transduction network is then of importance, giving account for how the external stimuli is detected, processed, and transmitted to reach the desired target. Several researchers have been addressing quantitatively how much information can be transmitted in the signal transduction networks [2–4]. The last step of signaling pathways involves the gene expression regulation by some transcription factors (TFs). The amount of gene product, i.e., the output, will depend on the information content of the TF signal that reach the *cis*-regulatory system (CRS) of the target gene, which must decode such information and generate the response. In this sense, some gene has been reported to respond with different expression patterns to distinct stimuli [5–8]. The expression level of the target gene is controlled by individual molecules interacting with regulatory regions of the CRS. Thus, any mesoscopic description of gene expression regulation must take into account the intrinsic noise associated to the discreteness of the binding and unbinding events. This noise, as well as the TF signal fluctuations, impact in the information transmission capacity of the CRS [4]. There is a growing interest to understand the constraints to downstream information propagation imposed by noisy input signals [4,9–15], which goes beyond the noise propagation in transcriptional cascades [16–19]. The information theory provides quantitative tools to deal with the information content of a signal and its transmission through noise channels [20]. These measures have been recently used to study information transmission in single-gene cascades both theoretically [10,12–14], as well as experimentally [15]. While in Ref. [10] the authors assume Gaussian models in the simplest gene activation motif, Hu *et al.* consider a noisy input signal arising from a simple birth-death process that regulates the transition rates of a two-state promoter switch [12,13].

As the output expression level depends not only on the input signal, but also on the architecture of the CRS, which determines how the TF stimuli are transmitted, we found it interesting to study the information transmission beyond the naive two-state promoter switch. In this direction is also the work of Rieckh and Tkačik, who proposed quantify the information transmission by the mutual information measure of a downstream gene with multiple internal states [14]. They found that internal states can reduce the information transmission capacity of the CRS, but in the case of cooperative regulation the system can outperform the channel capacity of two-state models [14]. However, the approach used in Ref. [14] is valid only for a small noise regime, when the probability distributions needed to compute the mutual information can be approximated by Gaussian distributions. Such approximation restricts the study to unimodal inputs. On the other hand, it has been shown that in the presence of cooperative binding the output response can also be associated to bimodal distributions [21].

Since cooperativity can play an important role in the information transmission capacity of the CRS, we are interested here to study the information transmission in a system where unimodal or bimodal input signals regulate cooperatively the many-state CRS of the downstream gene. In this paper, we take advantage of the spectral method [9,22] to exactly calculate the steady-state solution of the master equation describing our model, which allows us to compute the mutual information between input and output signal without

*monteoli@fisica.unlp.edu.ar
†ldiambra@gmail.com

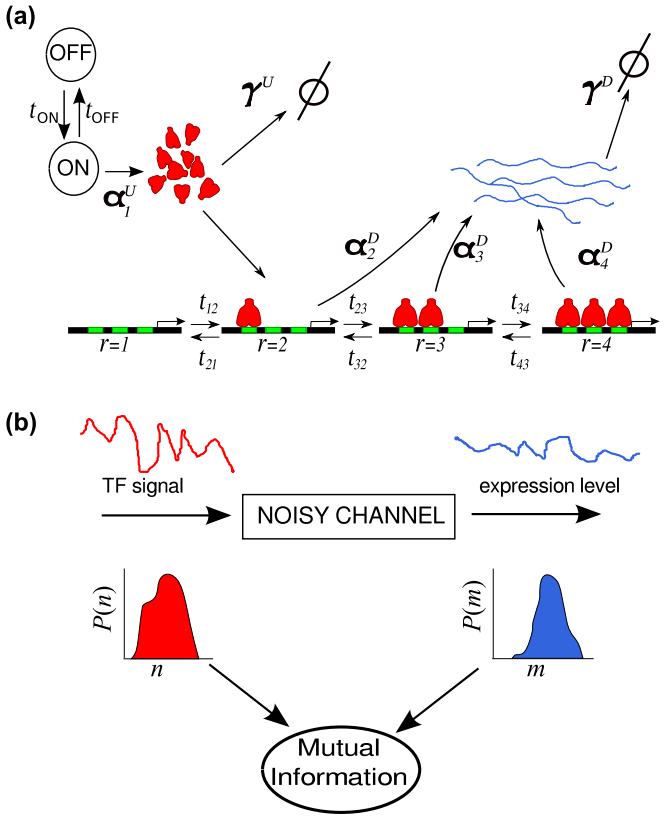

FIG. 1. (a) Two-gene cascade model, where TFs (red proteins) are synthesized at rate α_1^U by an upstream gene when it is in its ON state. TFs can bind cooperatively to the regulatory binding sites (green boxes) on the promoter of the downstream gene, whose expression rates α_r^D depend on the promoter state r. (b) Information transmission is measured by the Mutual Information between the probability distribution of TFs (input signal) and the probability distribution of transcripts associated to the downstream gene (output response).

approximation. In Sec. V, we present some results giving evidence that indeed cooperativity plays an important role on the information transmission issue. Furthermore, we show that when cooperativity is taken into account, its effects on information transmission depend on the mechanisms involved in the process of binding.

II. THE MODEL

We are interested in exploring the information transmission in the elementary building block of any gene regulatory network, that is, how the information encoded in the noisy input signal is transmitted through a gene subject to intrinsic chemical noise. In our model, the input signal arises from a nonregulated gene with two states, labeled by $s = 0, 1$. This gene is able to synthesize proteins at rate α_s^U, which degrade at rate γ^U. For the sake of simplicity we will consider that the inactive state, $s = 0$, is not able to synthesize proteins, i.e., $\alpha_0^U = 0$. Transitions between s states occur at rates $t_{\rm ON}$ and $t_{\rm OFF}$ as indicated on Fig. 1. The number of free proteins generated by this gene is labeled by n. This protein plays the role of the TF that regulates the gene response of the downstream gene (see Fig. 1). Notice that, for simplicity, we do not explicitly consider the intermediate mRNA of the nonregulated gene. The CRS of the regulated gene possesses a certain degree of complexity necessary to study the role of cooperativity on the information transmission in the single step gene cascade described above. In this sense, the CRS includes three functionally identical binding sites for the same TF, which renders into four states, denoted by $r = 1, 2, 3$, and 4 representing CRS states with zero, one, two, and three sites occupied, respectively, as illustrated in Fig. 1. TFs can bind to regulatory sites with a probability which is proportional to the TF concentration following the law of mass action for elementary reactions $t_{r,r+1} = nk_{r,r+1}$. TF unbinding events depend only on the kinetic constants $t_{r+1,r} = k_{r+1,r}$. We consider that only CRS states with one or more bounded TFs are able to synthesize mRNAs at a state-dependent rate, α_r^D. The number of transcripts produced by the regulated gene at time t will be denoted by m, and it degrades at a rate γ^D. Thus, our model is a cascade composed of two genes which from now on we call upstream and downstream genes.

To model a Hill-type response curve due to a cooperative binding process, we consider that the production rate of transcripts increases linearly with the occupancy number. In particular, we have set $\alpha_r^D = (r-1)\alpha$ for $r = 1, 2, 3$, and 4.

The model above has many parameters. However, we can show that the kinetic rates $k_{r,r+1}$ and $k_{r+1,r}$ can be written in terms of only three. To this end, let us consider first the same model without cooperativity, where the principle of detailed balance establishes

$$\frac{k^o_{r,r+1}}{k^o_{r+1,r}} = e^{-\Delta G_{\rm DNA}/RT}, \quad \text{for} \quad r = 1, 2, 3, \tag{1}$$

where $\Delta G_{\rm DNA}$ is the free energy of binding a TF to any binding site, $k^o_{r,r+1}$ represents the transition rate from state r to state $r+1$ when there is no interaction between TFs ($k^o_{r+1,r}$ represents the rate of reverse transition), R is the gas constant, and T is the absolute temperature. If there is cooperativity due to interaction between TFs, the total free energy involved is $\Delta G_{\rm DNA} + \Delta G_I$, where ΔG_I is the free energy of interaction between two TF molecules. We found useful to define the cooperativity intensity ε, as $\varepsilon = \mathrm{e}^{-\frac{\Delta G_I}{RT}}$. Thus, in presence of interaction between TFs, we have

$$\frac{k_{r,r+1}}{k_{r+1,r}} = e^{-\Delta G_{\rm DNA}/RT} e^{-z_r \Delta G_I/RT}, \tag{2}$$

where z_r represents the number of interactions. If we now assume that each new bound TF interacts with all TFs already bound to the DNA sites, then $z_r = r - 1$ for $r = 1, 2, 3$:

$$\frac{k_{r,r+1}}{k_{r+1,r}} = \varepsilon^{(r-1)} \frac{k^o_{r,r+1}}{k^o_{r+1,r}}. \tag{3}$$

As we assumed that the regulatory sites are identical, we can now introduce the combinatorial effect of the three sites and write $k^o_{r,r+1} = (\mathcal{N} - r + 1)p$ and $k^o_{r+1,r} = rq$, where p defines the probability per time unit that a single TF molecule binds to a regulatory site, and q is the probability per time unit that a single TF molecule unbinds from an occupied site. $\mathcal{N}$ is the number of binding sites in the CRS, which here was set to $\mathcal{N} = 3$. This number of sites is enough to make the cooperativity effects more apparent without adding unneeded complexity.

Relationship Eq. (3) leaves an extra degree of freedom, because the interaction between TFs can increase the ability for the recruitment of new TF for DNA binding, or it can diminish the unbinding rate. As pointed out in a previous work [23], cooperativity happens following two nonexclusive mechanisms. One of them, the recruitment mechanism, takes place when the already bounded TFs increase the ability for new TF recruitment for DNA binding, increasing the binding rates. In this case, the kinetic rates for the downstream gene can be written as

$$k_{r,r+1} = \varepsilon^{(r-1)}(4-r)p, \tag{4}$$

$$k_{r+1,r} = rq. \tag{5}$$

On the other hand, for the stabilization mechanism, which occurs when TF interaction diminishes the unbinding rate $k_{r+1,r}$, we have

$$k_{r,r+1} = (4-r)p, \tag{6}$$

$$k_{r+1,r} = \varepsilon^{(1-r)}rq. \tag{7}$$

Thus, these relationships allow us to write the kinetic rates of the CRS in terms of solely three parameters: the binding rate p, the unbinding rate q, and the cooperativity intensity ε. This model was deposited in SBML format on the BioModels database [24] and assigned the identifier MODEL1705160000.

We consider that all processes mentioned above are stochastic and each is described by an independent Poisson process. For this system, the state is specified by four stochastic variables: the state s of the upstream gene, the number n of free TFs, the state r of the CRS associated to the downstream gene, and the resulting number m of transcripts. The probability to find the system in state (s, n, r, m) at time t will be denoted by $P^{s,r}_{n,m}(t)$. The temporal evolution of this probability is governed by the following master equation:

$$\begin{aligned}\dot{P}^{s,r}_{n,m} &= \alpha^U_s\left(P^{s,r}_{n-1,m} - P^{s,r}_{n,m}\right)\\ &+\gamma^U\left[(n+1)P^{s,r}_{n+1,m} - nP^{s,r}_{n,m}\right]\\ &+\alpha^D_r\left(P^{s,r}_{n,m-1} - P^{s,r}_{n,m}\right)\\ &+\gamma^D\left[(m+1)P^{s,r}_{n,m+1} - mP^{s,r}_{n,m}\right]\\ &+\sum_{s'r'} K^T_{s',r'}P^{s',r'}_{n,m}\\ &+(n+1)\sum_{s'r'} K^F_{s',r'}P^{s',r'}_{n+1,m}\\ &+\sum_{s'r'} K^B_{s',r'}P^{s',r'}_{n-1,m}.\end{aligned} \tag{8}$$

The first two terms on the right-hand side of Eq. (8) describe the production and degradation of proteins generated by the upstream gene, while the third and fourth terms describe the production and degradation of the products generated by the downstream gene. The last three terms, with the matrices K^T, K^F, and K^B, take into account the transitions between states of up or downstream genes. The first of these is the one with matrix K^T, defined by

$$K^T = \begin{pmatrix} T-nK^F_1 & -K^B_1 & 0 & 0\\ 0 & T-nK^F_2 & -K^B_2 & 0\\ 0 & 0 & T-nK^F_3 & -K^B_3\\ 0 & 0 & 0 & T\end{pmatrix}, \tag{9}$$

which has two parts. One describes the internal transitions of the upstream gene through the matrix T, which is defined by

$$T = \begin{pmatrix} -t_{\mathrm{ON}} & t_{\mathrm{OFF}}\\ t_{\mathrm{ON}} & -t_{\mathrm{OFF}}\end{pmatrix}. \tag{10}$$

The other part, which involves the matrices $K^F_r = k_{r,r+1}\mathbf{1}_{2x2}$ and $K^B_r = k_{r+1,r}\mathbf{1}_{2x2}$ for $r = 1, 2, 3$, represents the binding and unbinding of free TFs on the binding sites of the CRS of the downstream gene through its transition rates $k_{r+1,r}$ and $k_{r+1,r}$ for $r = 1, 2, 3$. All zeros in Eq. (9) represent 2×2 matrices with zero entries. The same is true for all other zero entries on the following matrices. Finally, in the following two last terms, with matrices K^F and K^B defined by

$$K^F = \begin{pmatrix} 0 & 0 & 0 & 0\\ K^F_1 & 0 & 0 & 0\\ 0 & K^F_2 & 0 & 0\\ 0 & 0 & K^F_3 & 0\end{pmatrix} \tag{11}$$

and

$$K^B = \begin{pmatrix} 0 & K^B_1 & 0 & 0\\ 0 & 0 & K^B_2 & 0\\ 0 & 0 & 0 & K^B_3\\ 0 & 0 & 0 & 0\end{pmatrix}, \tag{12}$$

are described transitions in the CRS of the downstream gene which alter the the amount of free proteins n [25]. These two terms of our master equation make it differ from that of Mugler *et al.* (Eq. 138 in Ref. [22]), which do not take into account this fact.

Alternatively, one could have considered the total number of TFs as the stochastic variable n_{tot}. However, such an approach neglects the effect of bound molecules, which can affect the downstream information transmission, because the promoter is sensing only the free number of TFs.

Finally, time-dependent solutions for master equations are very difficult to obtain even in simpler models. Nevertheless, we are here interested in the steady-state solution of Eq. (8), denoted by $P^{*s,r}_{n,m}$. From now on all quantities such as probabilities, mean values, variances, etc., will be those corresponding to the steady state. Thus, to avoid making our notation cumbersome we drop the * from it.

III. THE MUTUAL INFORMATION

The presence of noise constraints how precisely changes in the TF level influence the information propagation to a gene controlled by a complex CRS. A way to quantify this transference is through the mutual information $\mathcal{M}$ between probability distributions associated with the input signal and

the response, $P(n)$ and $P(m)$, respectively, which is defined as [20]

$$\mathcal{M}(n;m) = \sum_{n,m} P(n,m) \log_b \left[\frac{P(n,m)}{P(n)P(m)} \right], \quad (13)$$

where $P(n,m) = \sum_{s,r} \hat{P}^{s,r}_{n,m}$ is the probability to find the system with n regulatory proteins and m transcripts, regardless of the internal states of each promoter, whereas $P(n)$ and $P(m)$ are the marginal probabilities $P(n) = \sum_{m,s,r} \hat{P}^{s,r}_{n,m}$ and $P(m) = \sum_{n,s,r} \hat{P}^{s,r}_{n,m}$. When the base $b = 2$, the units of the $\mathcal{M}$ measure is given in bits. Thus, $\mathcal{M}$ is the Kullback-Leibler divergence between two particular probability distributions: the joint probability $P(n,m)$ and the one obtained under the assumption of independence $P(n) \times P(m)$ [26,27]. The mutual information can be equivalently defined by: $\mathcal{M}(n;m) = S[n] + S[m] - S[n,m]$, where $S[X]$ is the entropy associated to the random variable X.

In the following section, we present the spectral method we used to compute $P^{s,r}_{n,m}$ and the marginal probabilities, following Ref. [22] so as to render the present paper as self contained as possible.

IV. THE SPECTRAL METHOD

We begin by defining a generating function $G_{s,r}(x,y) = \sum_{n,m} P^{s,r}_{n,m} x^n y^m$ over the complex variables x and y. As in Ref. [22], we use a representation that proves more convenient, writing the generating function with states indexed by $|n,m\rangle$, $|G_{s,r}\rangle = \sum_{n,m} P^{s,r}_{n,m} |n,m\rangle$, with inverse transform $P^{s,r}_{n,m} = \langle n,m|G_{s,r}\rangle$, and resorting to an operator formalism as in the quantum harmonic oscillator, $a_n^+|n\rangle = |n+1\rangle$ and $a_n^-|n\rangle = n|n-1\rangle$, with adjoint operators $\langle n|a_n^+ = \langle n-1|$ and $\langle n|a_n^- = (n+1)\langle n+1|$ for protein number n and similar relations for m. The more familiar form for the generating function is recovered by projecting the position space $\langle x|$ onto $|G_{s,r}\rangle$, taking into account that $\langle x|n\rangle = x^n$ with conjugate state $\langle n|x\rangle = 1/x^{n+1}$ and inner product $\langle f|f'\rangle = \oint \frac{dx}{2\pi i} \langle f|x\rangle\langle x|f'\rangle$ ensuring orthogonality of $|n\rangle$ states as can be verified using Cauchy's Theorem [22]. The same relations hold for y space. With these definitions, master Eq. (8) can be written as

$$|\dot{G_{s,r}}\rangle = -\hat{H}_{s,r}|G_{s,r}\rangle + \sum_{s',r'} \hat{\Omega}_{s',r'}|G_{s',r'}\rangle, \quad (14)$$

with

$$\hat{H}_{s,r} = b_n^+ b_{n,s}^- + \rho\, b_m^+ b_{m,r}^- \quad (15)$$

playing the role of a Hamiltonian operator and the operator matrix

$$\hat{\Omega}_{s,r} = \hat{K}^D + \hat{K}^B + \hat{K}^F \quad (16)$$

comprising all the CRS transitions. Operators b_n^+ and $b_{n,s}^-$ are shifted forms of the raising and lower protein number operators, $b_n^+ = a_n^+ - 1$, $b_{n,s}^- = a_n^- - \alpha_s^U/\gamma^U$, $b_m^+ = a_m^+ - 1$ and $b_{m,r}^- = a_m^- - \alpha_r^D/\gamma^D$, while $\rho = \gamma^D/\gamma^U$. As in the operator treatment of the harmonic oscillator in quantum mechanics, the raising and lower operators satisfy the commutation relation $[a_n^-, a_n^+] = 1$ and $a_n^+ a_n^-$ is a number operator, i.e., $a_n^+ a_n^-|n\rangle = n|n\rangle$. The same holds for a_m^+ and a_m^-. For details about this operator formalism, see Refs. [9,22]. Operator $\hat{K}^D$ was obtained from the corresponding matrix by replacing n by $a_n^+ a_n^-$ in K^D, while operators $\hat{K}^B$ and $\hat{K}^F$ were defined as $\hat{K}^B = a_n^+ K^B$ and $\hat{K}^F = a_n^- K^F$. The whole advantage of the method resides in the possibility to separate a diagonal part of the Hamiltonian operator $\hat{H}_{s,r}$ and use its *eigenvectors* to expand the generating function $|G_{s,r}\rangle$. Introducing the constant production rates α^U and α^D, and defining $b_n^- = a_n^- - \alpha^U/\gamma^U$ and $b_m^- = a_m^- - \alpha^D/\gamma^D$, we can split the Hamiltonian as $\hat{H}_{s,r} = \hat{H}_0 + \hat{H}_{1,s,r}$, with

$$\hat{H}_0 = b_n^\dagger b_n^- + \rho\, b_m^+ b_m^- \quad (17)$$

an operator that can be diagonalized, i.e.,

$$\hat{H}_0|j,k\rangle = (j + \rho k)|j,k\rangle, \quad (18)$$

where the $|j,k\rangle$ are its *eigenvectors*, and

$$\hat{H}_{1,sr} = b_n^+ \Gamma_s + \rho\, b_m^\dagger \Gamma_r \quad (19)$$

captures the deviations $\Gamma_s = b_{n,s}^- - b_n^- = \alpha^U - \alpha_s^U$ and $\Gamma_r = b_{m,r}^- - b_m^- = \alpha^D - \alpha_r^D$ of the constant production rates α^U and α^D we have introduced from the state-dependent production rates α_s^U and α_r^D of our model.

Expanding the generating function in the *eigenvectors* of $\hat{H}_0$,

$$|G^{s,r}\rangle = \sum_{j,k} G^{s,r}_{j,k}\, |j,k\rangle, \quad (20)$$

Eq. (14) takes the form

$$\dot{G}^{s,r}_{j,k} = -(j+\rho k) G^{s,r}_{j,k} - \Gamma_s G^{s,r}_{j-1,k} - \rho \Gamma_r G^{s,r}_{j,k-1} + \sum_{s',r'} \sum_{j'} \langle j|\hat{\Omega}^{s,r}_{s',r'}|j'\rangle G^{s',r'}_{j',k}. \quad (21)$$

As transition rates depend on n, not m [see master Eq. (8)], the matrix elements of operator $\hat{\Omega}^{s,r}_{s',r'}$ need to be calculated only in j space, not in k. Equation (21) is subdiagonal in k and thus more efficient than master Eq. (8). Its steady-state solutions are constructed beginning with the null space of the resulting matrix equation for $k = 0$,

$$\sum_{s',r',j'} \langle j|\hat{\Omega}^{s,r}_{s',r'} - (j\delta_{j',j} + \Gamma_s \delta_{j',j-1})\delta_{s',s}\delta_{r',r}|j'\rangle G^{s',r'}_{j',0} = 0,$$

and then solved at each subsequent k using the result for $k-1$. Notice that the solution involves only matrix multiplication and the inversion of a $8J \times 8J$ matrix K times, where J and K are cutoffs in the eigenmode numbers j and k, respectively. Normalization is needed and comes from the fact that probability must be unity (see Ref. [22] for a detailed derivation). The decomposition of the master Eq. (8) into linear algebraic equations results in huge gains in efficiency over its direct solution.

The probability $P^{s,r}_{n,m}$ is found from the $G^{s,r}_{j,k}$ with the inverse transform

$$P^{s,r}_{n,m} = \sum_{j,k} \langle n|j\rangle G^{s,r}_{j,k} \langle m|k\rangle, \quad (22)$$

where the mixed products are calculated from the recurrence relations

$$(n+1)\langle n+1|j\rangle = (\alpha^U + n - j)\langle n|j\rangle - \alpha^U \langle n-1|j\rangle,$$
$$\alpha^U \langle j|n+1\rangle = (\alpha^U + n - j)\langle j|n\rangle - n\langle j|n-1\rangle, \quad (23)$$

initialized with $\langle 0|j\rangle = (-1)^j e^{-\alpha^U}$ and $\langle 1|j\rangle = (-1)^j e^{-\alpha^U}(\alpha^U - j)$ and $\langle j|0\rangle = (-\alpha^U)^j/j!$ and $\langle j|1\rangle = (-\alpha^U)^j(1 - j/\alpha^U)/j!$, respectively, and updated recursively in n. Similar relations hold for $\langle m|k\rangle$. The constant production rates α^U and α^D introduced to define our diagonal Hamiltonian $\hat{H}_0$ are parameters that can be tuned so as to facilitate numerical stability and convergence of the calculations [22]. Our calculations were robust for different values of the cutoffs J, K for eigenmodes j and k, and cutoffs N and M for n and m, and also for different values of parameters α^U and α^D, but the convergence proved faster when they were set to the mean values of the production rates for each gene; i.e., we set $\alpha^U = \frac{1}{2}\sum_s \alpha_s^U$ and $\alpha^D = \frac{1}{4}\sum_r \alpha_r^D$. In no case the cutoffs were greater than $N = 70$, $M = 30$, $J = 65$, $K = 25$ for all situations here studied, and for most $N = 30 - 40$ and $J = 25 - 35$ proved sufficient.

V. RESULTS

Our goal is to gain insight into the role of cooperativity on the (downstream) information transmission through a single-step gene cascade. In order to meet this goal, we have studied the behavior of the mutual information $\mathcal{M}$ in different scenarios combining the following conditions: (i) the regulatory input signal has associated an unimodal or bimodal probability distribution; (ii) different relationships between the kinetic rates associated with the CRS and the rates of production and degradation of the transcript of the downstream gene; (iii) the CRS of the downstream gene is operating under recruitment or stabilization mechanisms; (iv) different noise levels associated with the input signal.

To consider the effects of different input probability distribution features on $\mathcal{M}$, we have selected two sets of parameter values for the kinetics of the upstream gene in such a way that the regulatory input signals associated with the unimodal and bimodal distributions have the same mean value $\bar{n}$ and noise level (measured as the Fano Factor $F_n = \frac{\sigma_n^2}{\bar{n}}$). This is accomplished by setting adequately the kinetics rates $t_{\rm ON}$, $t_{\rm OFF}$ and the TF production and degradation rates α_1^U and γ^U as the ones obtained for the isolated upstream gene, which can be analytically studied, as indicated in Appendix A. In this way, one can investigate how differently the features of the input signal affect the information transmission. Figure 2(a) depicts a unimodal (blue squares) and a bimodal (red disks) probability distribution associated with the regulatory input signals used as stimuli of the downstream gene. These probability distributions where obtained with the parameter values $\alpha_1^U = 3.5$, $t_{\rm ON} = 0.2087$, and $t_{\rm OFF} = 0.5218$ (unimodal distribution), and $\alpha_1^U = 1.5$, $t_{\rm ON} = 0.044$, and $t_{\rm OFF} = 0.022$ (bimodal distribution); $\gamma^U = 0.1$ in both cases. With these parameter values, the mean value and noise of the input signal are the same for both the unimodal and bimodal cases ($\bar{n} = 10$ and $F_n = 4$). Table I lists the values of the model parameters used in this study.

As done for the upstream gene, parameter values of the downstream gene were set considering it isolated. Thus, as for a fixed number of binding sites the steepness of the response curve is determined by the cooperativity intensity ε, we have studied the mutual information varying ε. However, ε also affects the dissociation constant K_d of the response curve.

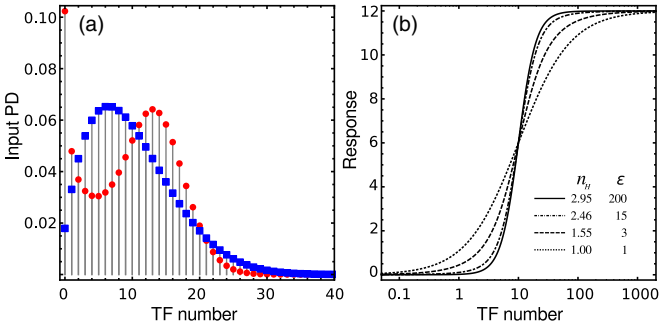

FIG. 2. (a) Unimodal and bimodal probability distributions for the isolated upstream gene product obtained using the parameters values $\alpha_1^U = 3.5, \gamma^U = 0.1, t_{\rm ON} = 0.2087$, and $t_{\rm OFF} = 0.5218$ (unimodal distribution, blue squares), and $\alpha_1^U = 1.5$, $\gamma^U = 0.1$ for $t_{\rm ON} = 0.044$ and $t_{\rm OFF} = 0.022$ (bimodal distribution, red disks). In both cases $F_n = 4$, while $\bar{n} = 10$, the same as the K_d of the curves response. (b) Regulatory function for the isolated downstream gene when parameters are $q = 0.75$, $\gamma^D = 0.25$, $\alpha_r^D = (r-1)\alpha$ with $\alpha = 1$; the value of the dissociation constant is fixed at $K_d = 10$. The response curves with different steepness ($n_H = 1$, 1.55, 2.46, and 2.95) correspond to different pairs of values $(\varepsilon, p) = (1, 0.075), (3, 0.025), (15, 0.005)$, and $(200, 0.000375)$.

To isolate the effect of cooperativity, we have chosen to vary parameters of the CRS in such a way that its dissociation constant is fixed at a particular value, taken to be the same as the mean value $\bar{n}$ of TFs, so that $K_d = 10$. This is accomplished by adjusting p simultaneously with ε as indicated in Appendix B, where we have also included the expression of the mean response. Parameters q, γ^D, and α_r^D stay unchanged. Figure 2(b) shows four response curves for the downstream gene with different Hill coefficients or steepnesses: $n_H = 1.0$ (with $\varepsilon = 1$ and $p = 0.075$, dotted line), $n_H = 1.55$ (obtained with $\varepsilon = 3$ and $p = 0.025$, dashed line), $n_H = 2.46$ (obtained with $\varepsilon = 15$ and $p = 0.005$ dot-dashed line), and $n_H = 2.95$ (obtained with $\varepsilon = 200$ and $p = 0.000375$, solid line), when $q = 0.75, \gamma^D = 0.25, \alpha_1^D = 0, \alpha_2^D = 1, \alpha_3^D = 2$, and $\alpha_4^D = 3$. All these curves have the same dissociation constant $K_d = 10$ and the same $V_{\rm max} = 12$. Notice that cooperative mechanisms (stabilization or recruitment) do not alter these response curves but only the fluctuation level [23]. Besides considering the effect of steepness of the response curve on information transmission, we are also interested in the role played by

TABLE I. Range of parameter values used in the study.

Gene	Parameter	Value [range]	Units
Upstream	$t_{\rm ON}$	[0.00013, 333.3]	$\rm min^{-1}$
	$t_{\rm OFF}$	[0.000067, 166.6]	$\rm min^{-1}$
	α_1^U	1.5,3.5	$\rm min^{-1}$
	γ^U	0.1	$\rm min^{-1}$
	f	[0.01–10000]	dimensionless
	p	[0.000375–0.075]	$\rm min^{-1}$
Downstream	q	0.75	$\rm min^{-1}$
	ε	[1.0–200]	dimensionless
	α	1.0	$\rm min^{-1}$
	γ^D	0.25	$\rm min^{-1}$

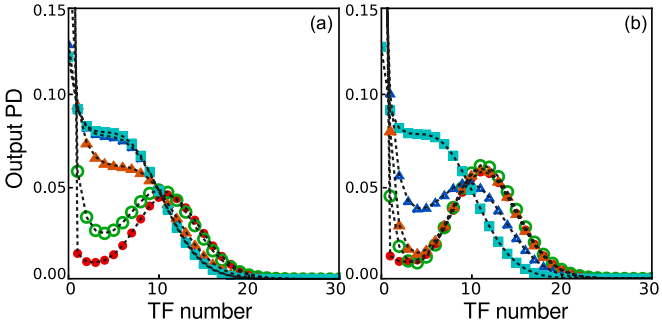

FIG. 3. Output probability distributions for the unimodal input signal depicted in Fig. 2(a). These distributions correspond to downstream-CRS with the same dose-response curve, but whose kinetic rates have been multiplied by a factor: $f = 0.1$ (red disks), $f = 1$ (green circles), $f = 10$ (orange filled triangles), $f = 100$ (blue open triangles), and $f = 10\,000$ (cyan squares). The CRS works with the stabilization (a) and the recruitment (b) cooperative mechanisms, using the parameters values $\varepsilon = 42$, $p = 0.001786$, while other parameters have the same values as those used in Fig. 2(b).

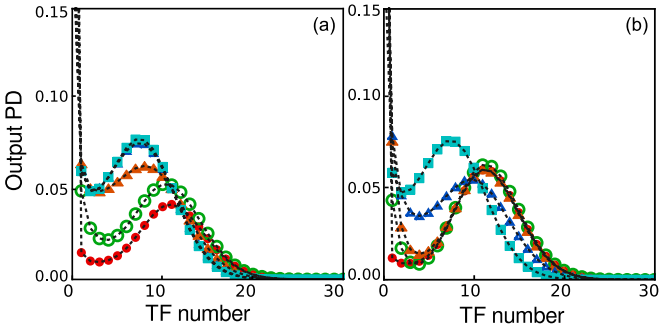

FIG. 4. Output probability distributions for the bimodal input signal depicted in Fig. 2(a). These distributions correspond to downstream-CRS with the same dose-response curve, but whose kinetic rates have been multiplied by a factor: $f = 0.1$ (red disks), $f = 1$ (green circles), $f = 10$ (orange filled triangles), $f = 100$ (blue open triangles), and $f = 10\,000$ (cyan squares). The CRS works with the stabilization (a) and the recruitment (b) cooperative mechanisms, using the parameters values $\varepsilon = 42$, $p = 0.001786$, while other parameters have the same values as those used in Fig. 2(b).

the kinetic rates of the CRS. By multiplying by a factor f the binding and unbinding rates p and q, one can explore the effects of slow to fast CRS dynamics on the information transmission. Notice that for the downtream gene factor f alters the fluctuation level of the output, but not the mean value of signal response, because the latter depends only on ratios rather than on individual kinetic rates [see Eq. (B2) in Appendix B].

We are now in a condition to study separately how different features of the downstream-CRS such as its kinetics, the associated n_H, the different mechanisms of underlying cooperativity on the one hand, and the different probability distributions of the input signal and its noise level on the other, may affect the information transmission characterized by the mutual information $\mathcal{M}$. Figure 3(a) illustrates ten different output distributions, associated with the transcript response level, in response to the unimodal input signal depicted in Fig. 2(a) (blue square symbols). These distributions correspond to a CRS that uses stabilization mechanism with $\varepsilon = 42$, $p = 0.001786$, while other parameters have the same values as those used in Fig. 2(b), but with the kinetic rates multiplied by a different factor: $f = 0.1$ (red disks), $f = 1$ (green circles), $f = 10$ (orange filled triangles), $f = 100$ (blue open triangles), and $f = 10\,000$ (cyan squares) [Fig. 3(a)]. In Fig. 3(b) the output distributions for the same unimodal input signal correspond to a CRS that use recruitment mechanism with the same parameter values as those used in the Fig. 3(a). Figure 4 illustrates the same corresponding output distributions but in response to the bimodal input signal depicted in Fig. 2(a) (red disk symbols). All output probability distributions have been computed with the spectral method as described on Sec. IV. In all cases illustrated in Figs. 3 and 4, the CRS mean response curves for the isolated downstream gene are the same. These examples illustrate that the overall output response (i.e., mean values and fluctuations) is not only determined by the input signal and the response curve of the downstream gene but also by the fluctuations associated with its CRS dynamics. This fact is a distinctive feature of the approach devised here in contrast with Ref. [14], where only response curves are taken into account. Furthermore, while the authors only consider Gaussian input signals, our approach extends to general input distributions.

In Fig. 5, we show the behavior of the mutual information when the cooperativity intensity ε changes keeping K_d of the curve response fixed, for the recruitment mechanism case, when the input signal has associated an unimodal (left panel) and bimodal (right panel) distribution. The different curves correspond to different values of factor f, which range from $f = 0.1$, for slow CRS dynamics, to $f = 10\,000$ for fast ones. Figure 6 illustrates the behavior of $\mathcal{M}$ versus ε for the stabilization mechanism case.

First, these figures show a different behavior for the mutual information $\mathcal{M}$ on ε when the downstream-CRS dynamics is slow compared to that of fast dynamics. For slow dynamics the information transference is remarkably small and its

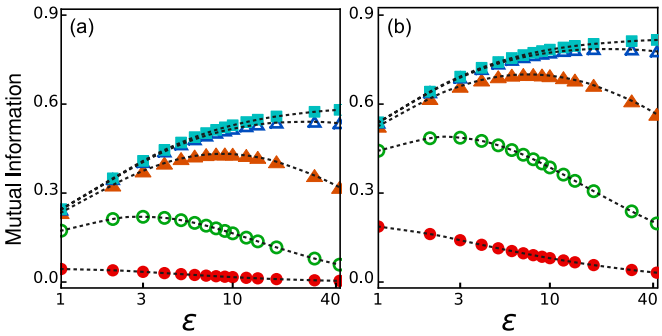

FIG. 5. Mutual information $\mathcal{M}$ vs. ε for the recruitment mechanism of the CRS when the input signal is the unimodal distribution depicted on Fig. 2 (left panel) and bimodal (right panel). Different symbols label different values of parameter f, ranging from slow dynamics of the downstream gene to very fast ones: $f = 0.1$ (red disks), $f = 1$ (green circles), $f = 10$ (orange filled triangles), $f = 100$ (blue open triangles), and $f = 10\,000$ (cyan squares). Dotted lines are drawn to help the eye.

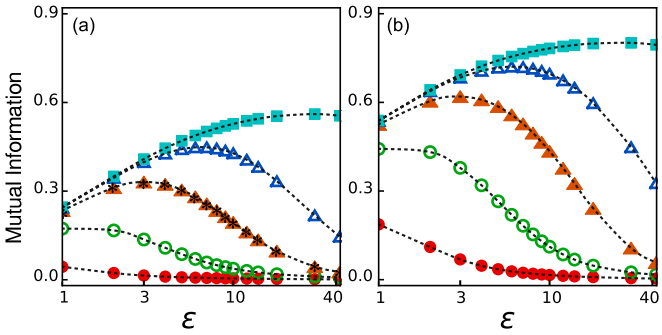

FIG. 6. Mutual information $\mathcal{M}$ vs. ε for the stabilization mechanism of the CRS when the input signal is the unimodal distribution depicted on Fig. 2 (left panel) and bimodal (right panel). Different symbols label different values of parameter f, ranging from slow dynamics of the downstream gene to very fast ones: $f = 0.1$ (red disks), $f = 1$ (green circles), $f = 10$ (orange filled triangles), $f = 100$ (blue open triangles), and $f = 10\,000$ (cyan squares). Asterisks correspond to the $\mathcal{M}$ computed using stochastic simulations with $f = 10$. Dotted lines are drawn to help the eye.

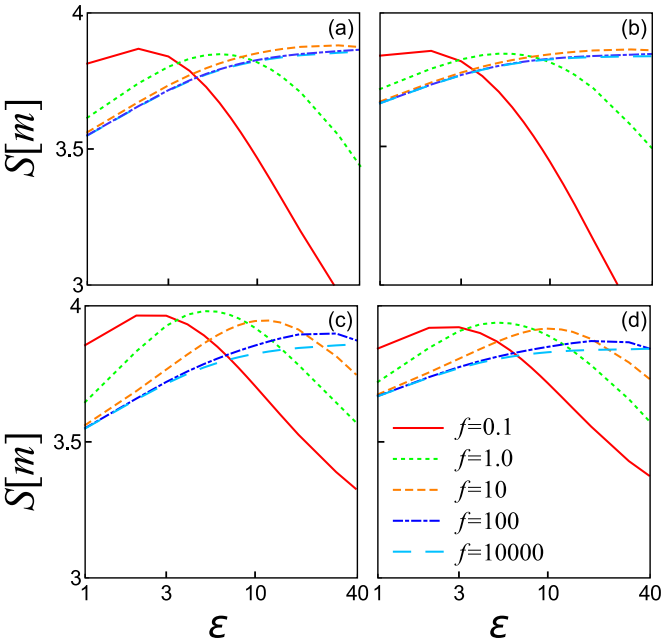

FIG. 7. Entropy of the output probability distributions $S[m]$ vs. ε for the recruitment mechanism when the input is unimodal (a) and bimodal (b), and for the stabilization mechanism when the input is unimodal (c) and bimodal (d). Different colors indicates different values of parameter f, ranging from slow dynamics of the regulated gene to very fast ones: $f = 0.1$ (red curves), $f = 1$ (green curves), $f = 10$ (orange curves), $f = 100$ (blue curves), and $f = 10\,000$ (cyan curves).

dependence on ε is that of a monotonous decreasing function (bottom curve). The same holds true for smaller values of f (not shown on the figures). For faster dynamics it first increases for low values of ε reaching a maximum and then decreases monotonously as a function of ε. This maximum happens at a larger value of ε as the CRS dynamics is faster, indicating that the relation of CRS kinetics to the kinetics of the upstream gene plays an import role. The decrease of the mutual information observed after reaching the maximum is due to the bimodal character of the output distribution promoted by the cooperative binding. This bimodal character is associated with the low entropy of the output distribution $S[m]$ at high cooperativity, see Fig. 7, but also to lower correlation between input and output signals. In this sense, Fig. 8 depicts three $P(n,m)$ histograms, computed from Gillespies simulations, for the stabilization cooperative mechanism for three different values of cooperative intensity: $\varepsilon = 1$ (a), $\varepsilon = 3$ (b), and $\varepsilon = 10$ (c), using $f = 10$ [orange filled triangles in Fig. 6(a)]. One can observe that the $P(n,m)$ corresponding to $\varepsilon = 1$ is wider than the one corresponding to $\varepsilon = 3$ where maximum on $\mathcal{M}$ occurs, while for $\varepsilon = 10$ and higher values the associated $P(n,m)$ has a higher skewness with a poor correlation with the input signal. Figure 9 illustrates the time courses of the stochastic simulations of the system in the same three parameter sets than those on Fig. 8.

Furthermore, for a fixed value of f this maximum occurs for a larger value of ε for recruitment mechanism of the downstream gene than for the stabilization mechanism independently of the distribution associated with of the input signal. By comparison of Figs. 5 and 6, we also notice that while the recruitment and stabilization cooperative mechanisms have a similar performance for low cooperativity ($\varepsilon < 3$), stronger differences are evident at higher values of ε. One can observe that, independently of the type of input signal, promoters operating with recruitment mechanism have higher information transmission capacity than those operating with stabilization mechanism. For example, $\mathcal{M}$ for the recruitment mechanism at $\varepsilon = 42$ and $f = 10$ is sixfold greater than $\mathcal{M}$ for the stabilization mechanism. This is due to the fact that the stabilization cooperative mechanism promotes a stronger bimodal response than the recruitment mechanism [21]. Thus, the existence of a maximum in the information transmission can be understood in terms of two contributions: (i) the cooperative binding affects the kinetics of the CRS through the Eqs. (4)–(7), increasing the $\mathcal{M}$ for low value of ε; (ii) the cooperative binding affects the output distribution, which goes from having an unimodal character to a bimodal one when ε increases, rendering a lower information transmission capacity. These are remarkable features if one is interested in promoters that maximize the information transmission.

There is also a striking difference between the behavior of $\mathcal{M}$ when the input signal is bimodal [Figs. 5(b) and 6(b)], compared to that corresponding to an unimodal input signal [Figs. 5(a) and 6(a)], even though both input signals have the same mean and Fano factor values. First of all, for the same set of parameters of the downstream gene, the $\mathcal{M}$ associated to a bimodal input signal is always higher than the one corresponding to an unimodal one. The difference of behavior for slow and fast dynamics remains similar, in the sense that for slow dynamics the mutual information decreases monotonically with ε, whereas for moderate and fast ones $\mathcal{M}$ reaches a maximum value, and this occurs for both input signals for the same value of ε, after which $\mathcal{M}$ decreases once again monotonously but in the case of bimodal input signal it remains always well above the value reached for the same ε for the unimodal input signal. This illustrates what we have pointed out above, that is, all the features of the output response

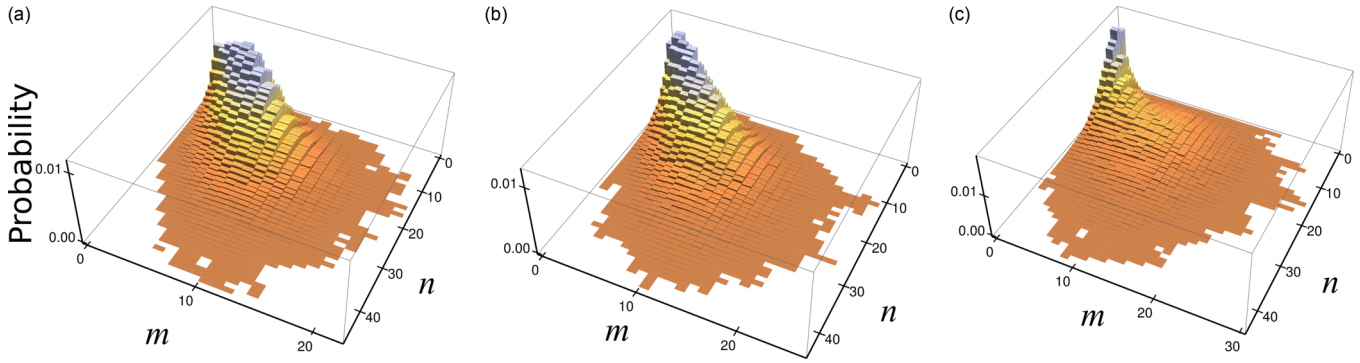

FIG. 8. Probability distributions $P(n,m)$ for the stabilization mechanism of the CRS, when the input signal is unimodally distributed around a mean value $\bar{n} = K_d = 10$ and with $F_n = 4$, and for three different values of the cooperativity intensity $\varepsilon = 1$ (a), $\varepsilon = 3$ (b), and $\varepsilon = 10$ (c). Other parameters values are those of the orange curve ($f = 10$) on Fig. 6(a).

play a role on the information transference, and not only the mean response, for if this last were the case, there would have been no difference among left and right panels on Figs. 5 and 6.

Until now we have considered only two input signals with the same noise level, as measured by the Fano factor ($F_n = 4$). Figure 10 depicts the mutual information $\mathcal{M}$ versus the entropy associated with the input signal, $S[n] = -\sum_n P(n) \log P(n)$, when the level of noise of the input signal is varied. The mean value is set at the value of the dissociation constant of the downstream gene, i.e., $\bar{n} = K_d = 10$, which is kept fixed. The different curves correspond to different values of ε, ranging from no cooperativity $\varepsilon = 1$ to $\varepsilon = 50$. The parameters of the downstream gene q, γ^D, and α_r^D are those of Fig. 2 and for the upstream gene we have set $\gamma^U = 0.1$ and $\alpha_1^U = 1.5$, which fixes the maximum value for F_n to 6. In order to keep constant the mean value of the input signal when F_n increases from 1 (unimodal distribution) to 6 (bimodal distribution), the rates t_{ON} and t_{OFF} are decreasing according to Eq. (A1), as detailed in Appendix A. These plots show that the entropy associated with the input signal $S[n]$ has a biphasic behavior: it first increases until 4.5, due to an increase of the second moment of the distribution, but when the bursting nature of the expression and bimodality of the distribution become prominent, the entropy associated with the input signal begins to decrease. On the other hand, $\mathcal{M}$ increases almost linearly with the Fano factor, with the exception of the case with high cooperativity and the stabilization mechanism. In this sense, it is interesting to note the low performance of promoters operating stabilization mechanism at high ε values. The increment of the information transmission when $S[n]$ decreases can be understood in terms of the bursting character of the input, which enhances the information transmission. This is apparent in Fig. 11, which depicts the time course

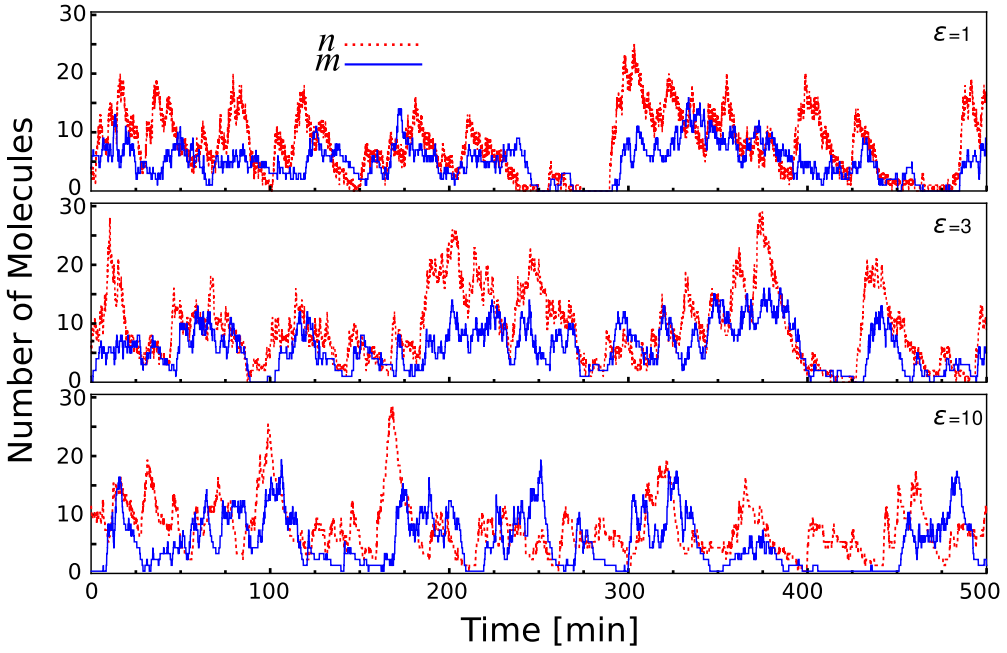

FIG. 9. Time courses of n (number of TFs) and m (transcript) corresponding to the histograms displayed in Fig. 8 obtained by Gillespies simulations.

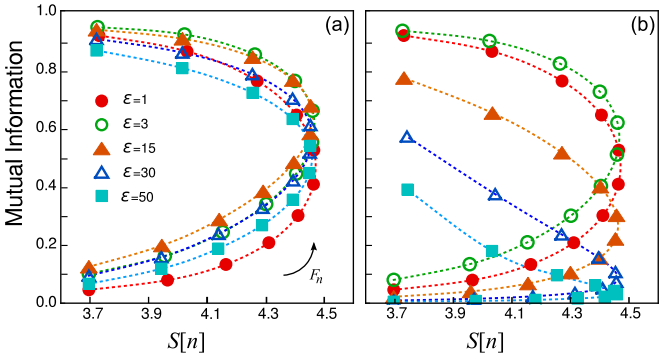

FIG. 10. Relationship between the Mutual information and the entropy of the input signal $S[n]$ for both cooperative mechanisms of the downstream gene: recruitment (a) and stabilization (b). The Fano factor F_n associated with the input signal increases from 1 to its maximum value for the selected parameters of the upstream gene (black arrow indicates the direction of increase), while its mean value is kept constant ($\bar{n} = K_d = 10$). The parameters of the downstream gene q, γ^D, and α_r^D are those of Fig. 2 and for the upstream gene we have set $\gamma^U = 0.1$ and $\alpha_1^U = 1.5$, which fixes the maximum value for F_n to 6. The different curves correspond to different values of ε, ranging from $\varepsilon = 1$ to $\varepsilon = 50$. Parameter p changes accordingly so as to keep K_d fixed.

of the stochastic simulations of the system when the noise of the input signal is increased. Again, promoters operating with the recruitment cooperative mechanism have higher information transmission capacity that those operating with the stabilization mechanism, independently on the noise level of the input signal.

VI. DISCUSSION AND CONCLUSION

Expression levels are the output of any regulatory network. This output depends on the topology of such regulatory network but also on the input signals. The passing on of the message through the gene regulation process can be severely affected by the chemical noise due the low copy number of players involved in the transcription processes. Despite the growing interest to understand how noisy input signals can regulate downstream switches, there are few theoretical approaches in the specialized literature addressing this issue. Among them we can mention the work of Hu *et al.*, which, by considering input signals arising from a birth-death process, explores the switching dynamics of the two-state downstream gene [12,13]. They found that increasing the fluctuation level in the input signal does not necessarily imply an increase in the output variation, as one could expect from the static approaches that consider correlations between input and output signals [11,17,28]. On the other hand, and from a static point of view, the seminal work of Rieckh and Tkačik considers the mutual information computation in the case of downstream genes with a three-state CRS [14]. They found that adding extra internal states can reduce the channel capacity of the CRS in relation to the two-state model. However, in the case of cooperative regulation, the system can outperform the information transmission of a two-state CRS [14]. This approach, which uses an analytic but approximated treatment, may not correctly capture the impact of noise on the information transmission process beyond the small-noise regime [14]. In any case, even when most studies support the idea of gene expression as a bursting dynamical process [29–31], very little is known about the information transmission of bursting input signals.

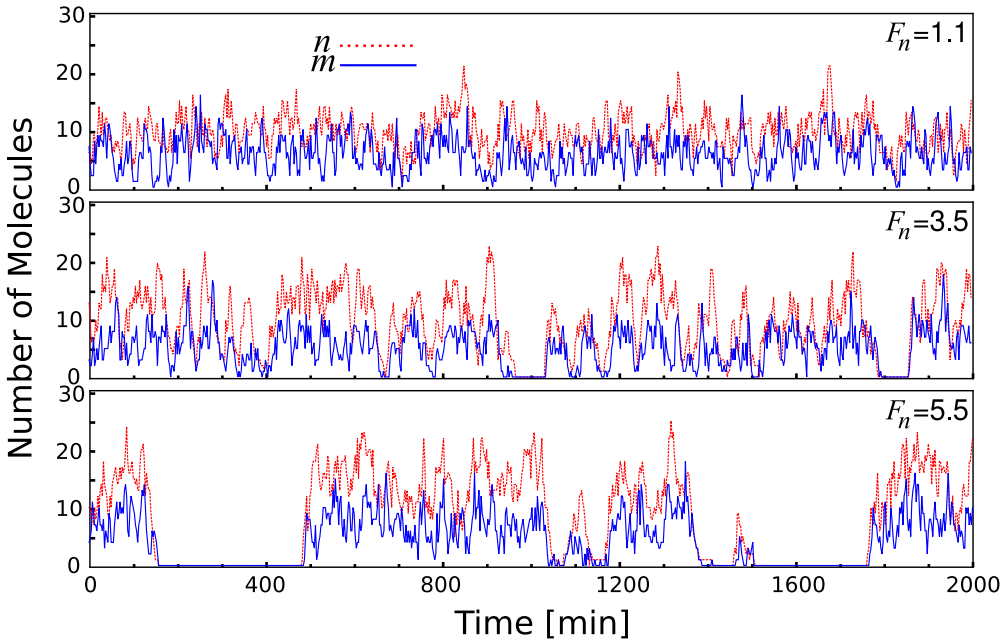

FIG. 11. Time courses of n (number of TFs) and m (transcript) for the gene cascade operating with the recruitment mechanism, $\varepsilon = 3$ and $f = 10$ [green curve of Fig. 10(b)] obtained by Gillespies simulations. Top panel corresponds to low value of $S[n]$ and $F_{=}1.1$ ($t_{\rm ON} = 3.267$, $t_{\rm OFF} = 1.633$), middle value of $S[n]$ and $F_{=}3.5$ ($t_{\rm ON} = 0.0667$, $t_{\rm OFF} = 0.0333$), Bottom panel low value of $S[n]$ and $F_{=}5.5$. ($t_{\rm ON} = 0.0074$, $t_{\rm OFF} = 0.0037$). The parameters of the downstream gene q, γ^D, and α_r^D are those of Fig. 2 and for the upstream gene we have set $\gamma^U = 0.1$ and $\alpha_1^U = 1.5$. Parameter p changes accordingly so as to keep $K_d = \bar{n} = 10$ fixed.

Furthermore, the effect of cooperative binding, which has been associated to bursting responses [21], on information transmission has not been addressed in previous studies. In this paper, taking advantage of the spectral method formalism, we computed exactly the probability distribution associated with both the input signal and the output response of the basic building block of any gene regulatory pathway, and we evaluated the associated mutual information. Our model allows us to explore not only a broad range of bursting kinetics inputs but also bursting outputs facilitated by the cooperative binding. We found that the recruitment cooperative mechanism has associated higher information transmission than the stabilization mechanism. The mutual information increases when the kinetic rates of the promoter increases, which becomes thus able to follow the change of the input signal. We also found that an increment on the noise level of the input signal does not necessarily imply a decrement on the information transmission. In the example depicted in Fig. 10, we show evidence supporting that input noise (quantified by the Fano factor) can increase the mutual information. Furthermore, our results indicate that the mutual information presents a maximum as function of the cooperativity intensity. This is an interesting feature, because this parameter, linked with the interaction energy between TFs, could be tuned in order to optimize the information transmission. In fact, these maximums occur within the physiological range of ε, taking into account that $\varepsilon = 6$ corresponds to around $\Delta G_I = 1.0$ kcal/mol [32,33].

Even though the method used here provides more accurate results than previous ones, it is important to remark on the limitations of the present approach to quantify the information transmission. The more evident limitation is that we are considering a static relationship between input and output PDs, and many aspects of the switching dynamics (e.g., dwell time statistics) have been overlooked. Other aspect of the present approach is that we are quantifying the information transmission with the mutual information measure $\mathcal{M}(n;m)$, which basically quantify how the random variables n and m are independent. Unfortunately, this measure is symmetric under the exchange of n and m and consequently does not provide the directional sense of transmitted information. Other measures, as the proposed by Ref. [26], could be more suitable for the purpose of quantifying the information transmission; however, their computation poses a challenge for future works.

ACKNOWLEDGMENTS

D.M. acknowledges support as a researcher of CICPBA (Argentina) and L.D. acknowledges financial support from Consejo Nacional de Investigaciones Científicas y Técnicas, Project No. PIP 0597 (Argentina).

APPENDIX A

It is our desire to tune parameters of the upstream gene so as to have different probability distributions features (unimodal or bimodal) for the input signal and different levels of noise as measured by the Fano factor of its distribution, keeping its mean value fixed. With this in mind, we have analyzed the upstream gene separately. Thus, from the master equation of the isolated gene,

$$\dot{P}_n^s = \alpha_s^U\left(P_{n-1}^s - P_n^s\right) + \gamma^U\left[(n+1)P_{n+1}^s - nP_n^s\right] + \sum_{s'} T_{s,s'}P_n^{s'},$$

we can compute the mean $\bar{n}$ and Fano factor F_n at steady state in terms of its parameters α_s^U, γ^U and the kinetics rates t_{ON} and t_{OFF}. We can then invert the obtained relations to solve t_{ON} and t_{OFF} as a function of the production and degradation rates and the values of the mean and Fano factor:

$$t_{\mathrm{ON}} = \frac{\alpha_0^U\alpha_1^U - \gamma^U\bar{n}\left(\alpha_0^U + \alpha_1^U - \gamma^U(\bar{n}-1)\right) + \gamma^U\bar{n}F_n}{\gamma^U\bar{n}\left(\alpha_0^U - \alpha_1^U\right)(1-F_n)},$$

$$t_{\mathrm{OFF}} = -\frac{\gamma^U - \alpha_1^U}{\gamma^U - \alpha_0^U}t_{\mathrm{ON}}, \tag{A1}$$

which hold whenever

$$1 < F_n < 1 - \frac{\left(\alpha_0^U - \gamma^U\bar{n}\right)\left(\alpha_1^U - \gamma^U\bar{n}\right)}{\bar{n}(\gamma^U)^2}, \qquad \alpha_1^U \neq \alpha_0^U. \tag{A2}$$

Notice that by fixing the mean and Fano factor values of the upstream gene, we are still free to fix arbitrarily production and degradation rates so as to hold relations Eq. (A2); i.e., there is a whole range of parameters possible for the upstream gene that satisfy constraints imposed by fixing $\bar{n}$ and F_n. So, we take advantage of this freedom with the purpose of analyzing the effects on $\mathcal{M}$ of input signals with (*i*) the same mean and noise but different probability distributions features (unimodal or bimodal) or (*ii*) different levels of noise for a fixed mean value.

Case (*i*): We fix the mean to $\bar{n} = 10$ and the noise to $F_n = 4$ for the isolated upstream gene. Thus, when $\alpha_1^U = 3.5$, $\gamma^U = 0.1$, the kinetic rates obtained from Eqs. (A1) are $t_{\mathrm{ON}} = 0.2087$ and $t_{\mathrm{OFF}} = 0.5218$, yielding the unimodal distribution depicted in blue on Fig. 2(a), whereas if $\alpha_1^U = 1.5$, $\gamma^U = 0.1$ the resulting rates are $t_{\mathrm{ON}} = 0.044$ and $t_{\mathrm{OFF}} = 0.022$ with a bimodal distribution depicted in red on the same figure.

Case (*ii*): We fix the mean to $\bar{n} = 10$ and the production and degradation rates to $\alpha_1^U = 1.5$ and $\gamma^U = 0.1$, so Eq. (A2) yields the range of variation allowed for the Fano factor for this parameter, i.e., $1 < F_n < 6$. The kinetic rates t_{ON}, t_{OFF} will decrease accordingly with increasing Fano factor, as established by Eqs. (A1).

In Figs. 3–8, parameters of the upstream gene when in the cascade were set as the ones obtained for the isolated gene in *case* (*i*), as they study the behavior of $\mathcal{M}$ for two different input signals with the same mean and noise while varying parameters of the downstream gene as proposed on Appendix B, while in Fig. 10, parameters of the upstream gene when in the cascade were set as the ones obtained for the isolated gene on *case* (*ii*), as they study the behavior of $\mathcal{M}$ for input signals with the same mean, while varying its noise, for a fixed set of parameters of the downstream gene.

APPENDIX B

For the downstream gene, our purpose is to tune its parameters so as to set the CRS, when isolated, to have

response curves with different steepness n_H, but with the same K_d and maximum rate $V_{\max}$. Thus, we analyze the isolated downstream gene separately. From the corresponding master equation,

$$\dot{P}_m^r = \alpha_r^D\left(P_{m-1}^r - P_m^r\right) + \gamma^D\left[(m+1)P_{m+1}^r - mP_m^r\right] + \sum_{r'}\Omega_{r,r'}P_m^{r'}, \tag{B1}$$

with Ω comprising all the CRS transitions for this isolated gene,

$$\Omega = \begin{pmatrix} -nk_{12} & k_{21} & 0 & 0 \\ nk_{12} & -nk_{23}-k_{21} & k_{32} & 0 \\ 0 & nk_{23} & -nk_{34}-k_{32} & k_{43} \\ 0 & 0 & nk_{34} & -k_{43} \end{pmatrix}, \tag{B2}$$

where n is the number of TF molecules, and k_{ij} are determined through p, q, and ε, as indicated above by Eqs. (4) or (6), depending on the cooperative mechanism involved.

The mean response of the downstream gene to n molecules at steady state can be obtained from Eq. (B1), yielding

$$\bar{m}(n) = \frac{1}{\gamma^D}\sum_r \alpha_r^D \bar{P}^r, \tag{B3}$$

where $\alpha_r^D = (r-1)\alpha$ for $r = 1, 2, 3$, and 4, with $\alpha = 1$, and $\bar{P}^r$ is the marginal probability at steady state $\bar{P}^r = \sum_m \bar{P}_m^r$ given by

$$\bar{P}^1 = \frac{1}{n^3K_1K_2K_3 + n^2K_1K_2 + nK_1 + 1},$$

$$\bar{P}^2 = \frac{n}{n^3K_2K_3 + n^2K_2 + n + (K_1)^{-1}},$$

$$\bar{P}^3 = \frac{n^2}{n^3K_3 + n^2 + n(K_2)^{-1} + (K_1K_2)^{-1}},$$

$$\bar{P}^4 = \frac{n^3}{n^3 + n^2(K_3)^{-1} + n(K_2K_3)^{-1} + (K_1K_2K_3)^{-1}},$$

where K_r are the equilibrium constants $K_r = \frac{k_{r,r+1}}{k_{r+1,r}}$. Thus, $\bar{m}$ is a sigmoidal function of n. In the limit $\varepsilon \to \infty$, this function converges to the well-known Hill function. However, in any other case the sigmoidal response Eq. (B3) can be characterized by three parameters: (i) the saturation value $V_{\max}$, which is defined as $\lim_{n\to\infty}\bar{m}(n)$; (ii) the half-maximum concentration, also known as the dissociation constant K_d, defined as the n value at which $\bar{m}(n = K_d) = V_{\max}/2$; and (iii) the steepness n_H, which in the general case can be defined as

$$n_H = \frac{4}{V_{\max}}\frac{d\bar{m}(n)}{d(\ln n)}\Big|_{n=K_d}. \tag{B4}$$

We choose to vary parameters of the downstream gene in such a way that its dissociation constant K_d is fixed at a particular value of n, taken to be the mean value of the upstream one, $\bar{n}$. Thus, we adjust p while varying the cooperativity intensity ε so as to keep this selected value of K_d fixed while changing the steepness of the regulation function steadily. Parameters q, γ^D, and α_r^D stay unchanged.

[1] B. Alberts, A. Johnson, J. Lewis, M. Raff, K. Roberts, and P. Walter, *Molecular Biology of the Cell*, 6th ed. (Garland Science, New York, 2002).
[2] T. Shibata and K. Fujimoto, Proc. Natl. Acad. Sci. USA **102**, 331 (2005).
[3] B. Hu, W. J. Rappel, and H. Levine, Phys. Rev. E **90**, 032702 (2014).
[4] R. Cheong, a. Rhee, C. J. Wang, I. Nemenman, and A. Levchenko, Science **334**, 354 (2011).
[5] J. E. Purvis and G. Lahav, Cell **152**, 945 (2013).
[6] N. Hao and E. K. O'Shea, Nat. Struct. Mol. Biol. **19**, 31 (2012).
[7] E. Batchelor, A. Loewer, C. Mock, and G. Lahav, Mol. Syst. Biol. **7**, 488 (2011).
[8] L. Cai, C. K. Dalal, and M. B. Elowitz, Nature **455**, 485 (2008).
[9] A. M. Walczak, A. Mugler, and C. H. Wiggins, Proc. Natl. Acad. Sci. USA **106**, 6529 (2009).
[10] F. Tostevin and P. R. Ten Wolde, Phys. Rev. Lett. **102**, 218101 (2009).
[11] G. Tkacik, C. G. Callan, and W. Bialek, Proc. Natl. Acad. Sci. USA **105**, 12265 (2008).
[12] B. Hu, D. A. Kessler, W. J. Rappel, and H. Levine, Phys. Rev. Lett. **107**, 148101 (2011).
[13] B. Hu, D. A. Kessler, W. J. Rappel, and H. Levine, Phys. Rev. E **86**, 061910 (2012).
[14] G. Rieckh and G. Tkačik, Biophys. J. **106**, 1194 (2014).
[15] A. S. Hansen and E. K. O'Shea, eLife **4**, e06559 (2015).
[16] J. M. Pedraza and A. van Oudenaarden, Science **307**, 1965 (2005).
[17] J. Paulsson, Nature **427**, 415 (2004).
[18] M. B. Elowitz, A. J. Levine, E. D. Siggia, and P. S. Swain, Science **297**, 1183 (2002).
[19] S. Hooshangi, S. Thiberge, and R. Weiss, Proc. Natl. Acad. Sci. USA **102**, 3581 (2005).
[20] T. M. Cover and J. A. Thomas, *Elements of Information Theory* (Wiley, New York, 2005).
[21] P. S. Gutierrez, D. Monteoliva, and L. Diambra, PLoS One **7**, e44812 (2012).
[22] A. Mugler, A. M. Walczak, and C. H. Wiggins, Phys. Rev. E **80**, 041921 (2009).
[23] P. S. Gutierrez, D. Monteoliva, and L. Diambra, Phys. Rev. E **80**, 011914 (2009).
[24] N. Le Novère, B. Bornstein, A. Broicher, M. Courtot, M. Donizelli, H. Dharuri, L. Li, H. Sauro, M. Schilstra, B. Shapiro, J. L. Snoep, and M. Hucka, Nucleic Acids Res. **34**, D689 (2006).
[25] R. Grima, D. R. Schmidt, and T. J. Newman, J. Chem. Phys. **137**, 035104 (2012).
[26] T. Schreiber, Phys. Rev. Lett. **85**, 461 (2000).
[27] L. Diambra, Phys. Rev. E **64**, 035202 (2001).

[28] S. Tănase-Nicola, P. B. Warren, and P. R. ten Wolde, Phys. Rev. Lett. **97**, 068102 (2006).
[29] I. Golding, J. Paulsson, S. M. Zawilski, and E. C. Cox, Cell **123**, 1025 (2005).
[30] A. Raj, C. S. Peskin, D. Tranchina, D. Y. Vargas, and S. Tyagi, PLoS Biol. **4**, e309 (2006).
[31] D. M. Suter, N. Molina, D. Gatfield, K. Schneider, U. Schibler, and F. Naef, Science **332**, 472 (2011).
[32] M. Dellarole, I. E. Sánchez, and G. de Prat Gay, Biochemistry **49**, 10277 (2010).
[33] G. K. Ackers, A. D. Johnson, and M. A. Shea, Proc. Natl. Acad. Sci. USA **79**, 1129 (1982).